Materials Advances

ROYAL SOCIETY OF CHEMISTRY

COMMUNICATION

View Article Online
View Journal | View Issue

Cite this: *Mater. Adv.*, 2024, 5, 8439

Received 3rd July 2024,
Accepted 9th October 2024

DOI: 10.1039/d4ma00674g

rsc.li/materials-advances

Synthesis of colloidal Pd nanoparticles immobilised on poly(*N*-vinylacetamide): characterisation and application in catalysis†

Kazuki Tabaru,[a] Kanji Okada,[a] Tatsuki Nagata,[a] Takeyuki Suzuki,[b] Hiromitsu Sogawa,[a] Fumio Sanda,[a] Takeshi Watanabe[c] and Yasuhi Obora *[a]

We immobilised colloidal palladium nanoparticles on poly(*N*-vinylacetamide). The polymer and the immobilised Pd NPs were characterised with characterisation methods such as transmission electron microscopy, dynamic light scattering, thermogravimetric analysis, Fourier-transform infrared spectroscopy, X-ray absorption spectroscopy, and X-ray photoelectron spectroscopy. Finally, we tested catalytic applications under Suzuki–Miyaura cross-coupling reaction conditions.

Metal nanoparticles (M NPs) less than 100 nm in size have emerged as useful materials for various applications owing to quantum effects including optical, electronical, and thermal properties.[1] To expand applications of M NPs, immobilisation is an important method to modify the base material.[2] In particular, the development of supports for M NPs to improve durability in catalytic applications has become a major field of research.[3] Moreover, supports for M NPs may assist in catalytic reactions owing to the presence of adjacent M NPs and synergic interactions with the surface of their supports.[4,5] For example, hydrogen spillover is a migration event of absorbed species between different inorganic surfaces, such as M NPs on metal oxide supports, which contributes to effective catalysis.[6] Alternatively, the presence of acidic and basic sites may result in a corporative catalytic activity with neighbouring M NPs on metal oxide supports.[7] The tailoring of chemical and physical properties of catalyst supports and surfaces allows for the design of the local environments around a catalytic centre and higher-order structures to provide conditions suitable for efficient catalysis. Modification with organic chemicals is often effective because the choice of organic molecules and the installation of different functional groups allows direct tuning of the chemical and physical properties of M NPs. Surfaces that are molecularly modified by an ionic liquid phase can immobilise M NPs to create systems with efficient catalytic activity in hydrogenation.[8,9] The development of polymer-immobilised catalysts has also been intensively studied because of the ease with which their properties can be modified.[10–12] The development of polymer-based supports has led to a versatile platform for M NPs, which may enable lower catalyst loading, continuous flow reactions, and aqueous phase catalysis.[13–15] Therefore, the development of new platforms to immobilise M NPs would be highly desirable for applications in catalysis to maximise catalytic activity toward organic transformations.

Our group previously reported the synthesis of a variety of M NPs (Fe, Cu, Ru, Pd, Ir, Pt, and Au) based on a liquid phase reduction method using *N*,*N*-dimethylformamide (DMF), which has a role as a protectant, reductant, and solvent.[16–18] These DMF-stabilised M NPs were active in catalytic reactions such as cross-coupling reactions, hydrogen borrowing reactions, and other transformations, exhibiting high catalytic activities at low catalyst loading in comparison with conventional methods.[19–22] Most recently, our group has also succeeded in immobilisation of DMF-stabilised Pd NPs onto organic supports such as poly(4-ethynylaniline) and nitrogen doped carbon nanodots.[23–26]

In the present study, we have demonstrated immobilisation of Pd NPs on a vinyl polymer bearing amide side chains to give a Pd NPs-immobilised poly(*N*-vinylacetamide) (Pd NPs-PNVA). The resulting polymer was soluble in water and alcohol and exhibited a catalytic activity for the Suzuki–Miyaura cross-coupling reaction under aqueous conditions. Furthermore, the Pd NPs-PNVA demonstrated catalyst recycling at least four times with no deterioration of the catalytic activity. The major focus of this study was to characterise the Pd NPs-PNVA in terms of their particle size and chemical properties including chemical bonding and oxidation states. Additionally, we investigated the catalytic

[a] *Department of Chemistry and Materials Engineering, Faculty of Chemistry, Materials and Bioengineering, Kansai University, Suita, Osaka 564-8680, Japan. E-mail: obora@kansai-u.ac.jp*
[b] *Comprehensive Analysis Center, SANKEN, The University of Osaka, Mihogaoka, Ibaraki, Osaka 567-0047, Japan*
[c] *Japan Synchrotron Radiation Research Institute, 1-1-1 Kouto, Sayo, Hyogo 679-5198, Japan*

† Electronic supplementary information (ESI) available. See DOI: https://doi.org/10.1039/d4ma00674g

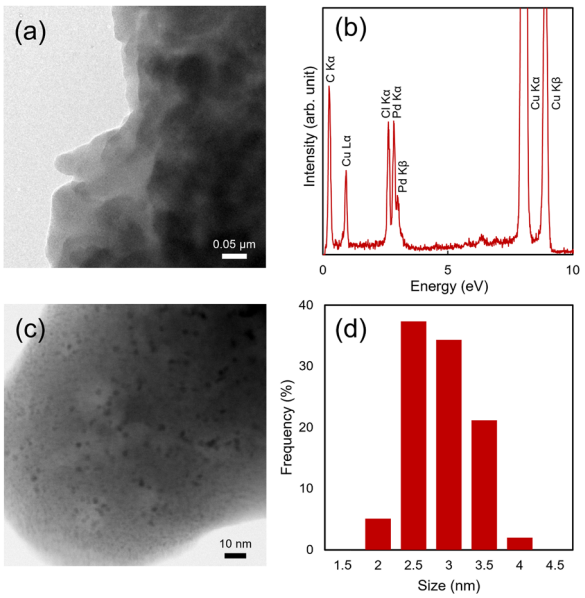

Fig. 1 (a) TEM image of the Pd NPs-PNVA (b) EDS plots (c) STEM image of the Pd NPs-PNVA (d) Size distribution of the Pd NPs-PNVA.

performance of the Pd NPs-PNVA in Suzuki–Miyaura cross-coupling reactions.

The Pd NPs-PNVA was synthesised from DMF-stabilised Pd NPs and PNVA (M_n = 12 000, $Đ$ = 3.2), prepared by previously reported methods.[19,27] The experimental details can be found in the ESI.†

First, the Pd NPs-PNVA was characterised by electron microscopy (Fig. 1). Fig. 1a shows a transmission electron microscope (TEM) image of the Pd NPs-PNVA. The polymer containing Pd element was analysed by energy-dispersive X-ray spectroscopy (EDS) (Fig. 1b). Additionally, induced coupled plasma atomic emission spectroscopy (ICP-AES) confirmed the presence of Pd and quantitative analysis found a Pd content of 0.55 wt% associated with the polymer. A high magnification scanning electron microscope (STEM) image of the Pd NPs-PNVA showed that the Pd NPs were evenly distributed on the PNVA (Fig. 1c). The average particle size of the Pd NPs on the PNVA was estimated to be 2.5 nm, which was approximately the same that determined for the DMF-stabilised Pd NPs.[19]

Additionally, dynamic light scattering (DLS) analysis showed the size distribution of the PNVA including the Pd NPs in a solution phase (Fig. 2a). The average particle size of the Pd NPs-PNVA was estimated to be 12.4 nm, and the particle size was slightly larger than that before immobilisation (9.8 nm).

The Pd NPs-PNVA was characterised by thermogravimetric (TG) analysis (Fig. 2b). The 5% weight loss temperature of the Pd NPs-PNVA was 164 °C whereas that of the Pd NPs was 169 °C. This result can be attributed to liberation of residual DMF molecules (boiling temperature is 153 °C) from around the Pd NPs. Subsequently, the slope of the TG curves for both the Pd NPs and the Pd NPs-PNVA decreased at 300 °C, indicating that the liberation of DMF was complete. Alternatively, the 5% weight loss temperature of PNVA was 334 °C, and the weight loss of the Pd NPs-PNVA also progressed from approximately 330 °C. These results suggested that the Pd NPs-PNVA exhibited notable stability as Pd NPs platforms compared to the Pd NPs protected simply by DMF molecules, which can be attributed to the thermal stability of PNVA as a protectant.

Fourier-transform infrared (FT-IR) spectra of the Pd NPs-PNVA exhibited IR absorption peaks around 3280 and 1560 cm^{-1} corresponding to stretching and vibration of N–H bonds, respectively (Fig. 2c).[28] A strong absorption band at approximately 1650 cm^{-1} indicated the presence of carbonyl groups from the amide polymer. There were no notable differences between the spectra of the Pd NPs-PNVA and PNVA.

To confirm the structure of Pd species in the PNVA, X-ray diffraction (XRD) measurement was carried out. However, XRD patterns of Pd species might be overlapped owing to the low Pd content compared to PNVA (Fig. S2, ESI†). Alternatively, solution-phase X-ray absorption spectroscopy (XAS) was performed to the local structure of the Pd NPs-PNVA. The Pd K-edge X-ray absorption near edge structure (XANES) profiles showed the oxidation state of Pd species for Pd foil, PdO, the Pd NPs, and the Pd NPs-PNVA (Fig. 3a). The absorption edge of the Pd NPs-PNVA was in a similar region to that of PdO and at

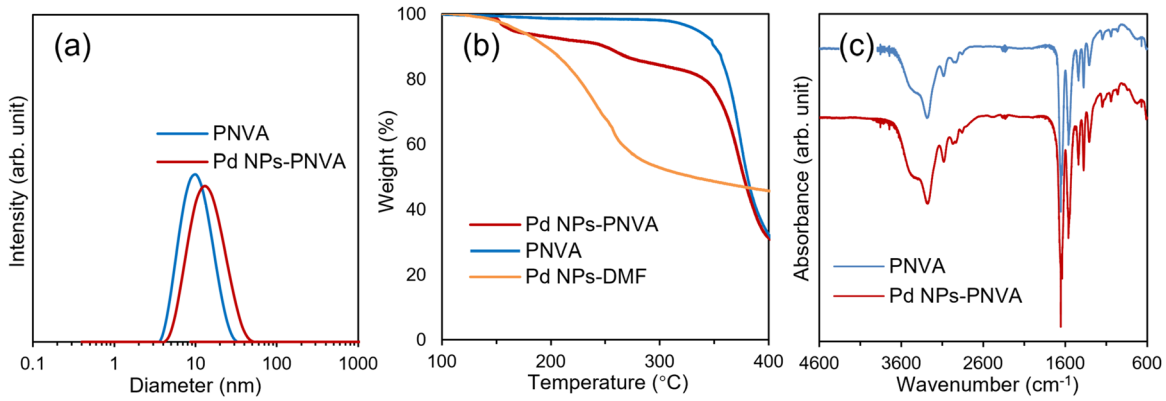

Fig. 2 (a) DLS size distribution curves of the Pd NPs-PNVA; (b) TG curves of PNVA, Pd NPs-DMF, and the Pd NPs-PNVA; (c) FT-IR spectra of PNVA and the Pd NPs-PNVA (KBr pellet).

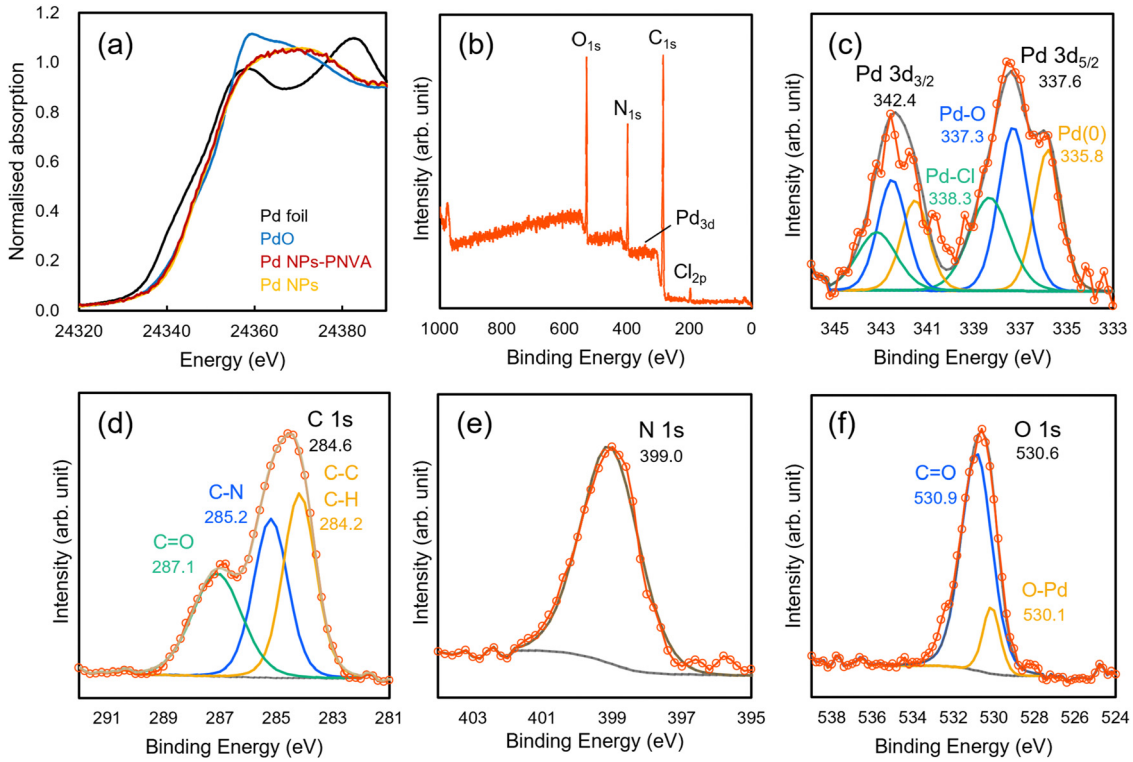

Fig. 3 (a) Solution-phase Pd K-edge X-ray absorption near edge spectra of the Pd NPs-PNVA; XPS profiles of the Pd NPs-PNVA (b) survey spectra, (c) Pd 3d region, (d) C 1s region, (e) N 1s region, and (f) O 1s region.

higher energy than that of Pd foil. This result indicates that the Pd(II) species were dominant in the Pd NPs-PNVA. No remarkable changes of the spectral shift and spectral shape were observed in comparison with Pd NPs.

Additionally, X-ray photoelectron spectroscopy (XPS) was performed to investigate the oxidation state of the surface of the Pd NPs-PNVA. Survey spectra detected the presence of Pd, C, N, O, and Cl on the material surface (Fig. 3b). The peak at 335.8 eV was attributed to metallic Pd on the support (Fig. 3c), and was slightly higher than that of Pd in the bulk (approximately 335.2 eV).[29–33] Other peaks at 337.3 and 338.3 eV were attributed to Pd(II) species including Pd–O and Pd–Cl, respectively.[30,34–37] The binding energies of these peaks were markedly increased compared with those of the DMF-stabilised Pd NPs with no support.[38,39] The high resolution spectra for C 1s, N 1s, and O 1s are shown in Fig. 3d–f. The C 1s spectrum was fitted to peaks at 284.2, 285.2, and 287.1 eV, representing C–C/C–H, C–N, and C═O bonds, respectively.[40–42] The peak in the N 1s region was located at 399.0 eV. The fitted O 1s spectra were assigned to Pd–O at 530.1 eV (ref. 29) and C═O at 530.9 eV.[40–42] These results were consistent with our FT-IR analysis of the bare PNVA.[28]

These characterisation results show that Pd NPs with a size of 2.5 nm were immobilised in the polymer network of PNVA, which formed particles as large as 12.4 nm. Pd(0) and Pd(II) species, including Pd–O and Pd–Cl bonds, were exposed on the particle surfaces, whereas inside the PdNPs-PNVA particles Pd(II) rather than Pd(0) species dominated. Additionally, the Pd NPs were not directly interacting with the functional groups of PNVA, as no spectral shift was observed in the FT-IR. Conversely, the peaks in the XPS of the Pd 3d region exhibited a notable shift to the higher binding energy. Therefore, these results indicated that the Pd NPs would be nested within the PNVA matrix.

Finally, we confirmed the catalytic activity of the Pd NPs-PNVA under the Suzuki–Miyara cross-coupling reaction. The reaction between iodobenzene (**1a**, 0.5 mmol) and 4-methylphenylboronic acid (**2a**, 1.5 equiv.) was performed in the presence of the Pd NPs-PNVA (20 mg, Pd content 0.55wt%, 0.2 mol%) and $CsCO_3$ (1.0 equiv.) in MeOH (2 mL) at 100 °C for 24 h, affording 4-methylbiphenyl (**3a**) in 77% GC yield (Scheme 1, entry 1). The use of K_2CO_3 (1.0 equiv.) instead of $CsCO_3$ was effective for this transformation providing the corresponding product in quantitative yield, where the catalyst turnover number was calculated to be 5.0×10^2 (entry 2). Alternatively, when the reaction was carried out in mixed solvents with a 1 : 1 volume ratio of H_2O and *N*-methyl-2-pyrrolidone (NMP), both $CsCO_3$ and K_2CO_3 were effective base for this transformation (entries 3 and 4). The use of toluene or 1,4-dioxane resulted in moderate yields (entries 5 and 6). We also investigated the reaction of bromobenzene (**1b**, 0.5 mmol) and **2a** (1.5 equiv.) using Pd NPs-PNVA (20 mg) and $CsCO_3$ (1.0 equiv.) in MeOH (2 mL) at 100 °C for 24 h, providing **3a** in 32% GC yield (entry 7). The use of K_2CO_3 instead of $CsCO_3$ did not improve the product yield (entry 8). The Pd NPs-PNVA exhibited high catalytic activity in the combined aqueous solutions with either $CsCO_3$ or K_2CO_3 (entries 9 and 10). In this reaction, the use of toluene and 1,4-

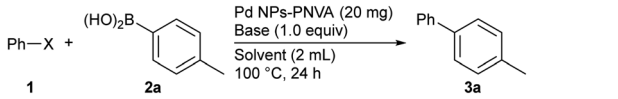

Entry	Ph-X	Base	Solvent	Conv (%) of **1**	Yield (%) of **3a**
1	**1a**	$CsCO_3$	MeOH	>99	77
2	**1a**	K_2CO_3	MeOH	>99	>99
3	**1a**	K_2CO_3	H_2O/NMP	>99	>99
4	**1a**	$CsCO_3$	H_2O/NMP	>99	>99
5	**1a**	K_2CO_3	Toluene	57	45
6	**1a**	K_2CO_3	1,4-Dioxane	71	67
7	**1b**	$CsCO_3$	MeOH	51	32
8	**1b**	K_2CO_3	MeOH	41	34
9	**1b**	$CsCO_3$	H_2O/NMP	>99	84
10	**1b**	K_2CO_3	H_2O/NMP	95	84
11	**1b**	K_2CO_3	Toluene	59	47
12	**1b**	K_2CO_3	1,4-Dioxane	68	43

Scheme 1 Pd NPs-PNVA-catalysed Suzuki–Miyaura cross-coupling reaction.[a] [a] Reaction conditions: Ph-X (**1**, 0.5 mmol), 4-methylphenylboronic acid (**2a**, 1.5 equiv.), base (1.0 equiv.), and solvent (2 mL) at 100 °C for 24 h. [b] Conversion and yield were determined by GC based on **1** used (*n*-tridecane as an internal standard).

dioxane decreased the product yield to 47% and 43%, respectively (entries 11 and 12).

We investigated the scope of substrates with the Pd NPs-PNVA-catalysed Suzuki–Miyaura cross-coupling reaction (Scheme 2). Under the reaction conditions of Scheme 1 entry 3, **3a** was obtained in 94% isolated yield (Scheme 2, entry 1). The use of

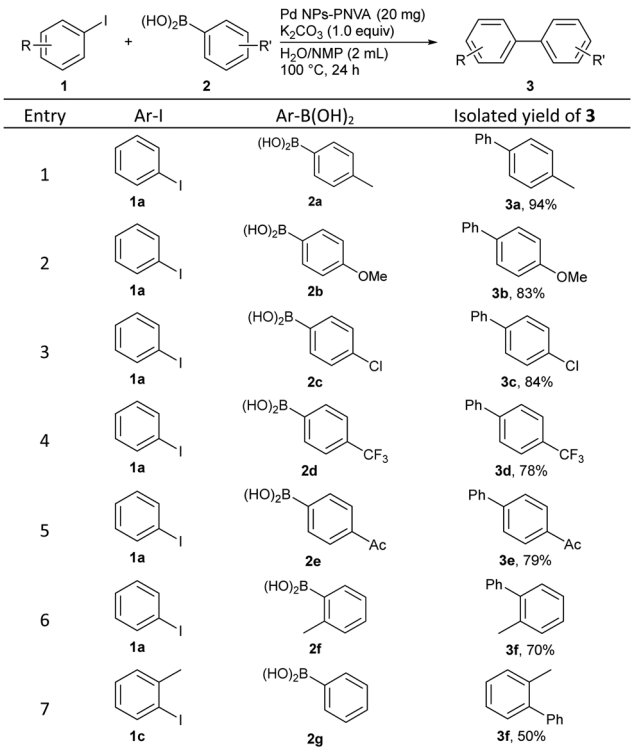

Scheme 2 Substrate scope Pd NPs-PNVA-catalysed Suzuki–Miyaura cross-coupling reaction[a] [a] Reaction conditions: Ar–I (**1**, 0.5 mmol), Ar–$B(OH)_2$ (**2**, 1.5 equiv.), K_2CO_3 (1.0 equiv.), and H_2O/NMP (2 mL) at 100 °C for 24 h.

4-methoxyphenylboronic acid (**2b**) with an electron-donating group smoothly yielded the corresponding product (**3b**) in 83% yield (entry 2). Alternatively, the reaction with phenylboronic acid bearing electron-withdrawing groups including Cl, CF_3, and acetyl (Ac) groups were tolerated under these conditions to give biphenyl derivatives in 78–84% yields (entries 3–5). To investigate the effect of steric hindrances under these conditions, we used ortho-substituted iodoaryl and arylboronic acid. The reaction between **1a** and 2-methylphenylboronic acid (**2f**) provided 2-methylbiphenyl (**3f**) in 70% (entry 6) whereas the reaction with 2-iodotoluene (**1c**) and phenylboronic acid (**2g**) yielded **3f** in 50% yield (entry 7). This indicated that the steric hindrance of aryl halide slightly interfered the oxidative addition of the catalyst.

To confirm recyclability of the Pd NPs-PNVA, catalyst recycling experiments were performed using **1a** with **2a** (Scheme S1, ESI†). First, the reaction of **1a** with **2a** in the presence of the Pd NPs-PNVA (20 mg), K_2CO_3, and the mixed solvent of H_2O with NMP gave **3a** in 92% GC yield. The catalyst was successfully recovered by extraction with hexane to remove the product and residual substrates. Subsequently, fresh substrates (**1a** and **2a**) and K_2CO_3 were added to the remaining catalyst. The second reaction provided **3a** in 90% GC yield. In the subsequent third and fourth catalyst recycling experiments, the corresponding product was obtained in high yield (See the ESI†), confirming the recyclability of the Pd NPs-PNVA under Suzuki–Miyaura cross-coupling reactions with no remarkable decrease in catalytic activity.

In conclusion, we immobilised Pd NPs on PNVA and characterised the physical and chemical properties of the material. The polymer was dispersed in solution as 12.4 nm particles associated with Pd NPs less than 3 nm in size. The immobilised Pd species mainly existed as Pd(II) species. Finally, the Pd NPs-PNVA exhibited catalytic activity under Suzuki–Miyaura cross-coupling reaction conditions. The catalyst was simply recovered by an extraction procedure and the catalytic activity was maintained at least four times. We believe our findings will benefit and expand the development of catalyst platforms based on M NP catalysts.

Data availability

The data supporting this article have been included as part of the ESI.†

Conflicts of interest

There are no conflicts to declare.

Acknowledgements

This work was supported by Japan Science and Technology Agency (JST) Support for Pioneering Research Initiated by the Next Generation (SPRING) (Grant Number JPMJSP2150), the Research Program for Next Generation Young Scientists of "Dynamic Alliance for Open Innovation Bridging Human,

Environment and Materials'' in ''Network Joint Research Center for Materials and Devices'', and the Kansai University Fund for Supporting Formation of Strategic Research Centers (University Initiative Type), 2024. We thank Mr Yosuke Murakami and Ms Nao Eguchi, SANKEN, The University of Osaka, for TEM, ICP-AES analyses. The synchrotron radiation experiments were performed at beamline BL14B2 of SPring-8 with the approval of the Japan Synchrotron Radiation Research Institute (Proposal 2022B1952).

Notes and references

1 D. Bera, L. Qian and P. H. Holloway, *Luminescent Materials and Applications*, John Wiley & Sons, Ltd, Chichester, UK, 2008, pp. 19–73.
2 Q.-L. Zhu and Q. Xu, *Chemistry*, 2016, **1**, 220–245.
3 D. Astruc, F. Lu and J. R. Aranzaes, *Angew. Chem., Int. Ed.*, 2005, **44**, 7852–7872.
4 L. Liu and A. Corma, *Chem. Rev.*, 2018, **118**, 4981–5079.
5 T. W. van Deelen, C. Hernández Mejía and K. P. de Jong, *Nat Catal.*, 2019, **2**, 955–970.
6 M. Xiong, Z. Gao and Y. Qin, *ACS Catal.*, 2021, **11**, 3159–3172.
7 H. Miura, M. Doi, Y. Yasui, Y. Masaki, H. Nishio and T. Shishido, *J. Am. Chem. Soc.*, 2023, **145**, 4613–4625.
8 L. Offner-Marko, A. Bordet, G. Moos, S. Tricard, S. Rengshausen, B. Chaudret, K. L. Luska and W. Leitner, *Angew. Chem., Int. Ed.*, 2018, **57**, 12721–12726.
9 A. Bordet and W. Leitner, *Acc. Chem. Res.*, 2021, **54**, 2144–2157.
10 N. E. Leadbeater and M. Marco, *Chem. Rev.*, 2002, **102**, 3217–3273.
11 Y. Uozumi and Y. M. A. Yamada, *Chem. Rec.*, 2009, **9**, 51–65.
12 S. Muratsugu, S. Shirai and M. Tada, *Tetrahedron Lett.*, 2020, **61**, 151603.
13 R. Hudson, G. Hamasaka, T. Osako, Y. M. A. Yamada, C.-J. Li, Y. Uozumi and A. Moores, *Green Chem.*, 2013, **15**, 2141–2148.
14 R. Hudson, H. R. Zhang, A. LoTemplio, G. Benedetto, G. Hamasaka, Y. M. A. Yamada, J. L. Katz and Y. Uozumi, *Chem. Commun.*, 2018, **54**, 2878–2881.
15 H. Miyamura, A. Suzuki, T. Yasukawa and S. Kobayashi, *J. Am. Chem. Soc.*, 2018, **140**, 11325–11334.
16 X. Liu, C. Li, J. Xu, J. Lv, M. Zhu, Y. Guo, S. Cui, H. Liu, S. Wang and Y. Li, *J. Phys. Chem. C*, 2008, **112**, 10778–10783.
17 H. Kawasaki, *Nanotechnol. Rev.*, 2013, **2**, 5–25.
18 T. Nagata and Y. Obora, *ACS Omega*, 2020, **5**, 98–103.
19 M. Hyotanishi, Y. Isomura, H. Yamamoto, H. Kawasaki and Y. Obora, *Chem. Commun.*, 2011, **47**, 5750–5752.
20 K. Tabaru, M. Nakatsuji, S. Itoh, T. Suzuki and Y. Obora, *Org. Biomol. Chem.*, 2021, **19**, 3384–3388.
21 M. Kobayashi, H. Yamaguchi, T. Suzuki and Y. Obora, *Org. Biomol. Chem.*, 2021, **19**, 1950–1954.
22 T. Nagata, T. Tanaka, X. Lin, R. Kondo, T. Suzuki, Y. Kanda, T. Toyao, K.-I. Shimizu and Y. Obora, *ChemCatChem*, 2022, **14**, e202101672.
23 S. Asada, A. Nito, Y. Miyagi, J. Ishida, Y. Obora and F. Sanda, *Macromolecules*, 2017, **50**, 4083–4087.
24 P. Suktanarak, T. Tanaka, T. Nagata, R. Kondo, T. Suzuki, T. Tuntulani, P. Leeladee and Y. Obora, *Bull. Chem. Soc. Jpn.*, 2020, **93**, 1164–1170.
25 M. Goto, M. Nakaoka, T. Nagata, T. Suzuki, H. Kawasaki, Y. Obora, H. Sogawa and F. Sanda, *J. Networkpolym.*, 2023, **44**, 275–285.
26 N. Kaittidanusorn, T. Nagata, M. Juthathan, K. Tabaru, N. Siengdung, P. Pienpinijtham, T. Tanaka, T. Suzuki, T. Tuntulani, P. Leeladee and Y. Obora, *Results Chem.*, 2024, **7**, 101398.
27 M. Akashi, E. Yashima, T. Yamashita, N. Miyauchi, S. Sugita and K. Marumo, *J. Polym. Sci., Part A: Polym. Chem.*, 1990, **28**, 3487–3497.
28 Y. Cai, M. Chen and X. Huang, *J. Rare Earths*, 2005, **23**, 230–234.
29 M. C. Militello and S. J. Simko, *Surf. Sci. Spectra*, 1994, **3**, 387–394.
30 R. V. Gulyaev, A. I. Stadnichenko, E. M. Slavinskaya, A. S. Ivanova, S. V. Koscheev and A. I. Boronin, *Appl. Catal., A*, 2012, **439–440**, 41–50.
31 C. He, J. Tao, Y. Ke and Y. Qiu, *RSC Adv.*, 2015, **5**, 66695–66703.
32 Y. Wang, X. Yang and J. Yu, *RSC Adv.*, 2017, **7**, 31850–31857.
33 X. Wang, J. Chen, J. Zeng, Q. Wang, Z. Li, R. Qin, C. Wu, Z. Xie and L. Zheng, *Nanoscale*, 2017, **9**, 6643–6648.
34 M. C. Militello and S. J. Simko, *Surf. Sci. Spectra*, 1994, **3**, 395–401.
35 J. C. Zhou, C. M. Soto, M.-S. Chen, M. A. Bruckman, M. H. Moore, E. Barry, B. R. Ratna, P. E. Pehrsson, B. R. Spies and T. S. Confer, *J. Nanobiotechnol.*, 2012, **10**, 18.
36 F. Bozon-Verduraz, A. Omar, J. Escard and B. Pontvianne, *J. Catal.*, 1978, **53**, 126–134.
37 M. C. Militello and S. J. Simko, *Surf. Sci. Spectra*, 1994, **3**, 402–409.
38 T. Nagata, T. Inoue, X. Lin, S. Ishimoto, S. Nakamichi, H. Oka, R. Kondo, T. Suzuki and Y. Obora, *RSC Adv.*, 2019, **9**, 17425–17431.
39 J. Ishida, M. Nakatsuji, T. Nagata, H. Kawasaki, T. Suzuki and Y. Obora, *ACS Omega*, 2020, **5**, 9598–9604.
40 C.-W. Chen, T. Serizawa and M. Akashi, *Chem. Mater.*, 1999, **11**, 1381–1389.
41 T. A. Gillam, C. K. Goh, N. Ninan, K. Bilimoria, H. S. Shirazi, S. Saboohi, S. Al-Bataineh, J. Whittle and A. Blencowe, *Appl. Surf. Sci.*, 2021, **537**, 147866.
42 E. Wulandari, K. Bilimoria, M. Krasowska, S. Al-Bataineh, D. Beattie, T. Gillam, W. Ge, J. D. Whittle, E. H. H. Wong and A. Blencowe, *Appl. Surf. Sci.*, 2023, **641**, 158422.